

Recent studies of kaonic atoms and nuclear clusters

Avraham Gal

Racah Institute of Physics, The Hebrew University, Jerusalem, Israel

Abstract

Recent studies of kaonic atoms, few-body kaonic quasibound states and kaonic nuclei are reviewed, with emphasis on implementing the subthreshold energy dependence of the $\bar{K}N$ interaction in chiral interaction models that are consistent with the SIDDHARTA K^- hydrogen data. Remarks are made on the possible role of the p -wave $\Sigma(1385)$ resonance with respect to that of the s -wave $\Lambda(1405)$ resonance in searches for strangeness $\mathcal{S} = -1$ dibaryons.

Keywords: kaon-baryon interactions, few-body systems, mesic nuclei, mesonic atoms

1. Introduction

Recent NLO chiral model calculations of near-threshold $\bar{K}N$ dynamics, reproducing the SIDDHARTA measurement of atomic K^- hydrogen $1s$ level shift and width [1], have been discussed by Hyodo [2]. The $\Lambda(1405)$ -induced strong energy dependence of the scattering amplitudes $f_{\bar{K}N}(\sqrt{s})$ arising in these calculations introduces a new feature into the analysis of K^- atomic and nuclear systems as realized for K^- atoms in the early 1970s [3, 4]. Thus, in nuclear matter, approximated for $A \gg 1$ by the lab system,

$$s = (\sqrt{s_{\text{th}}} - B_K - B_N)^2 - (\vec{p}_K + \vec{p}_N)^2 \leq s_{\text{th}} , \quad (1)$$

where $\sqrt{s_{\text{th}}} \equiv m_K + m_N$, B_K and B_N are binding energies, and where additional downward energy shift is generated by the momentum dependent term. Unlike in the free-space $\bar{K}N$ cm system where $(\vec{p}_K + \vec{p}_N)_{\text{cm}} = 0$, this term is found to contribute substantially in the lab system in realistic applications. Therefore, a reliable model extrapolation of $\bar{K}N$ amplitudes into subthreshold energies is mandatory in K^- atom and nuclear applications.

Below I give a brief overview of works on kaonic quasibound systems and kaonic atoms where subthreshold $\bar{K}N$ amplitudes were used in a physically

correct way during the last two years. It is shown how the energy dependence of these amplitudes, when translated into density dependence, leads to special patterns in kaonic systems. Finally, I focus attention to the recently proposed $I = 3/2$, $J^\pi = 2^+$ $\Sigma(1385)N$ dibaryon around the $\pi\Sigma N$ threshold [5] and suggest how to search for it in experiments that look for the $I = 1/2$, $J^\pi = 0^-$ $\Lambda(1405)N$ dibaryon, better known as K^-pp . In lieu of a concluding section, conclusions are marked in boldface throughout this review.

2. Few-body kaonic quasibound states

A prototype of such states is K^-pp which stands for $\bar{K}NN$ with isospin $I = 1/2$ and spin-parity $J^\pi = 0^-$, dominated by $I_{NN} = 1$ and s waves. A summary of few-body calculations of this system is given in Table 1 updating older versions in recent international conferences [6].

Table 1: Calculated K^-pp binding energies B & widths Γ (in MeV).

	chiral, energy dependent			non-chiral, static calculations			
	var. [7]	var. [8]	Fad. [9]	var. [10]	Fad [11]	Fad [12]	var. [13]
B	16	17–23	9–16	48	50–70	60–95	40–80
Γ	41	40–70	34–46	61	90–110	45–80	40–85

The listed calculations are $\bar{K}NN$ variational (var.) where the complex $\bar{K}N$ interaction accounts for the $\bar{K}N-\pi\Sigma$ two-body coupled channels but disregards $\bar{K}NN-\pi\Sigma N$ coupling, or fully coupled channels three-body Faddeev (Fad.). A more revealing classification of these calculations is according to whether or not the input two-body interactions are energy dependent. The table makes it clear that the binding energies calculated by using chiral, energy dependent interactions are considerably lower than those calculated using energy independent interactions, the reason for which is the marked difference between the $(\bar{K}N)_{I=0}$ interaction strengths which yield a quasibound state at ≈ 1420 MeV in the former case and at ≈ 1405 MeV in the latter case.

The recent calculations by Barnea et al. [7] include on top of K^-pp also the four-body $\bar{K}NNN$ quasibound states with $I = 0, 1$ and the $I = 0$ lowest $\bar{K}\bar{K}NN$ quasibound state. The calculations were done extending a nuclear hyperspherical basis to include \bar{K} mesons. The A -body wavefunctions were expanded in this complete basis and (real) ground-state binding energies

were computed variationally. Convergence was assessed by increasing systematically the size of the basis used. For input two-body interactions, the AV4' V_{NN} was used together with an effective energy-dependent complex $V_{\bar{K}N}$ [14] and a weakly repulsive $V_{\bar{K}\bar{K}}$ [15]. In single- \bar{K} configurations, $V_{\bar{K}N}$ was evaluated at subthreshold energies obtained by expanding Eq. (1) non-relativistically near $\sqrt{s_{\text{th}}}$:

$$\sqrt{s} = \sqrt{s_{\text{th}}} - \frac{B}{A} - \frac{A-1}{A}B_K - \xi_N \frac{A-1}{A} \langle T_{N:N} \rangle - \xi_K \left(\frac{A-1}{A} \right)^2 \langle T_K \rangle, \quad (2)$$

where $\xi_{N(K)} \equiv m_{N(K)}/(m_N+m_K)$, B is the total binding energy of the system and $B_K = -E_K$, T_K is the kaon kinetic energy operator in the total cm frame and $T_{N:N}$ is the pairwise NN kinetic energy operator in the NN pair cm system. This expression provides a self-consistency cycle by requiring that \sqrt{s} derived through Eq. (2) from the solution of the Schroedinger equation agrees with the value of \sqrt{s} used for the input $V_{\bar{K}N}(\sqrt{s})$. A similar expression was obtained for $\bar{K}\bar{K}NN$ configurations. The $\bar{K}N \rightarrow \pi Y$ widths of these few-body systems were evaluated using the expression

$$\frac{\Gamma}{2} \approx \langle \Psi_{\text{g.s.}} | -\text{Im } \mathcal{V}_{\bar{K}N} | \Psi_{\text{g.s.}} \rangle, \quad (3)$$

where $\mathcal{V}_{\bar{K}N}$ sums over all pairwise $\bar{K}N$ interactions. Expression (3) provides a good approximation owing to $|\text{Im } \mathcal{V}_{\bar{K}N}| \ll |\text{Re } \mathcal{V}_{\bar{K}N}|$ [14].

Results of self consistent calculations are shown in Fig. 1 with relevant thresholds marked in red horizontal lines. Since both $|\text{Re } V_{\bar{K}N}|$ and $|\text{Im } V_{\bar{K}N}|$ decrease upon going subthreshold [14], the self-consistently calculated binding energies (widths) come out typically 10 (10–40) MeV lower than when $V_{\bar{K}N}(\sqrt{s_{\text{th}}})$ is imposed. The $I = 1/2$ $\bar{K}NN$ g.s. corresponds to the most left-hand side ‘ K^-pp ’ calculation listed in Table 1. It lies only 4.3 MeV below the 11.4 MeV centroid of the $I = 0$ $\bar{K}N$ quasibound state, the latter value differing substantially from the value 27 MeV borrowed from the $\Lambda(1405)$ resonance in non-chiral calculations. The next two quasibound states shown in the figure are the lowest $I = 0$ and $I = 1$ $\bar{K}NNN$ quasibound states, the $I = 0$ state is the one predicted first by Akaishi and Yamazaki to be bound by over 100 MeV [16]. Finally, the calculated 32 MeV binding energy of $\bar{K}\bar{K}NN$ is substantially lower than the one advocated for it by Yamazaki et al. [17]. **With total binding energies of order 30 MeV calculated by Barnea et al. for the $A = 4$ kaonic clusters [7], there is little incentive to**

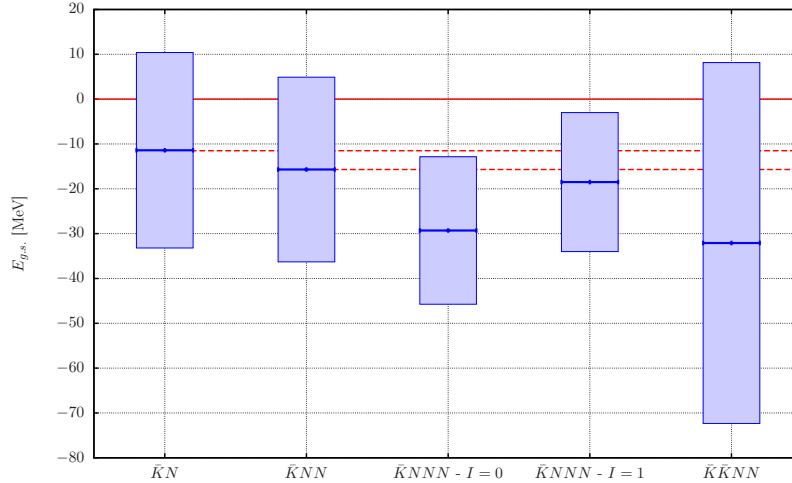


Figure 1: Calculated binding energies and $\bar{K}N \rightarrow \pi Y$ widths of \bar{K} and $\bar{K}\bar{K}$ few-body quasibound states [7] in MeV. Horizontal lines denote particle-stability thresholds and widths are represented by vertical bars.

argue that \bar{K} mesons offer a realization of strange hadronic matter in nature, more than Λ and Ξ hyperons do [18]. The widths exhibited in Fig. 1, of order 40 MeV for single- \bar{K} clusters and twice as much for double- \bar{K} clusters, are due to $\bar{K}N \rightarrow \pi Y$. Two-nucleon absorption widths $\Delta\Gamma_{\text{abs}}$ accounting for the poorly understood non-pionic processes $\bar{K}NN \rightarrow YN$ add $\Delta\Gamma_{\text{abs}}(K^-pp) \lesssim 10$ MeV in K^-pp [8] and ~ 20 MeV in the 4-body systems [7]. **Given the low binding energies and sizable widths in chirally motivated calculations, a clear identification of such near-threshold quasibound states in ongoing experimental searches is likely to be difficult.** For K^-pp , in particular, a \bar{K}^0d quasibound state contamination cannot be ruled out, with arguments for and against its presence that may be deduced from Refs. [19, 20] respectively.

3. Kaonic atoms

Here I review the latest kaonic atom calculation [21], using for input the recent Ikeda-Hyodo-Weise (IHW) NLO chiral K^-N subthreshold scattering amplitudes [22] which are constrained by the kaonic hydrogen SIDHARTA measurement [1]. Shown on the l.h.s. of Fig. 2 is the free-space

charge averaged K^-N c.m. subthreshold scattering amplitude $f_{K^-N}(\sqrt{s})$. Its substantial energy dependence was converted to density dependence by the expression

$$(\sqrt{s_\rho})_{\text{atom}} \approx \sqrt{s_{\text{th}}} - B_N(\rho/\bar{\rho}) - 15.1(\rho/\rho_0)^{2/3} + \xi_K(\text{Re } V_{K^-} + V_{\text{Coul}}(\rho/\rho_0))^{1/3} \quad (4)$$

(in MeV), obtained by taking the limit $A \gg 1$ in Eq. (2) where the nuclear kinetic energy was evaluated within the Fermi gas model, giving rise to a $\rho^{2/3}$ dependence, and the K^- kinetic energy was traded in favor of $\text{Re}V_{K^-} + V_{\text{Coul}}$ in the local density approximation. For atoms, $B_K = 0$ was assumed. The density dependence attached to B_N (where $\bar{\rho}$ is the *average* nuclear density) and to V_{Coul} ensures that the low-density limit is satisfied. The resulting self-consistent application of the constraint (4) in kaonic atom fits is shown on the r.h.s. of Fig. 2 where subthreshold K^-N energies probed by the self-consistently fitted K^- nuclear potential at threshold are plotted as a function of nuclear density in Ni and Pb. It is seen that the energy downward shift at 50% of central nuclear density amounts to ≈ 40 MeV.

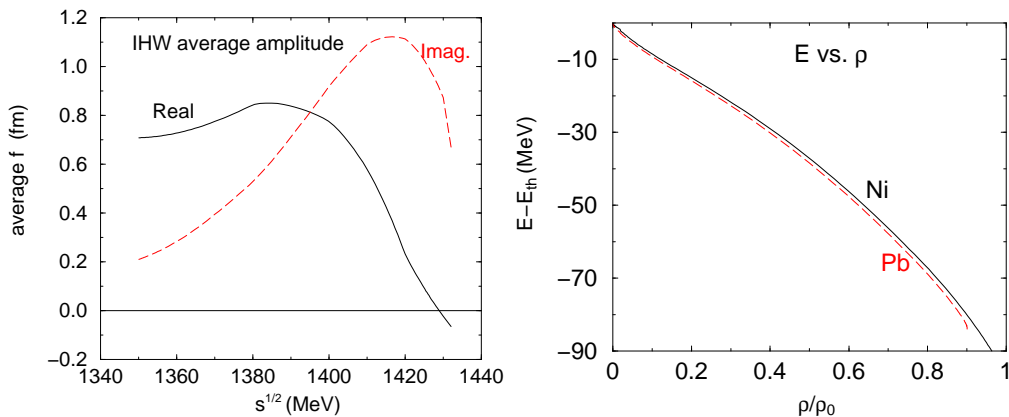


Figure 2: Left: the IHW cm scattering amplitude $f_{K^-N}(\sqrt{s}) = \frac{1}{2}(f_{K^-p}(\sqrt{s}) + f_{K^-n}(\sqrt{s}))$ [22]. Right: subthreshold K^-N energies probed by V_{K^-} as a function of nuclear density in Ni and Pb, calculated self consistently from the IHW-based best fit to kaonic atoms specified in Table 2.

The K^- nuclear potential employed in the kaonic atom fits is composed of two pieces, $V_{K^-}^{(1)}(\rho)$ and $V_{K^-}^{(2)}(\rho)$. The first one, $V_{K^-}^{(1)}(\rho)$, is derived from an underlying free-space chiral model. In Refs. [23, 24] in-medium amplitudes

were obtained directly by solving the in-medium coupled-channels Lippmann-Schwinger equations as a function of the nuclear density ρ , using separable interaction models by Cieplý and Smejkal [25], see for example Fig. 1 of Gazda and Mareš in these proceedings [26]. In the very recent kaonic atom analysis by Friedman and Gal [21] the free-space IHW cm amplitudes f were used as input in a multiple scattering approach [27] to generate in-medium cm amplitudes $\mathcal{F}_{K^-N}(\rho)$, dominated by Pauli correlations, viz.

$$\mathcal{F}_{K^-N}(\rho) = \frac{(2f_{K^-p} - f_{K^-n})\frac{1}{2}\rho_p}{1 + \xi(\rho)\tilde{f}_{I=0}\rho(r)} + \frac{f_{K^-n}(\frac{1}{2}\rho_p + \rho_n)}{1 + \xi(\rho)\tilde{f}_{I=1}\rho(r)}, \quad (5)$$

where $\tilde{f} = (\sqrt{s}/m_N)f$ is a lab amplitude, and $\xi(\rho) = 9\pi/4p_F^2$ with p_F the Fermi momentum. $V_{K^-}^{(1)}(\rho)$ is then given by

$$2\mu_K V_{K^-}^{(1)}(\rho) = -4\pi \tilde{\mathcal{F}}_{K^-N}(\rho). \quad (6)$$

Since absorptivities turn out to play a key role in the analysis of kaonic atoms, I demonstrate on the l.h.s. of Fig. 3 the ratio between the imaginary parts of $\mathcal{F}_{K^-N}(\rho)$ and $f_{K^-N}(\rho)$, plotted on a logarithmic density scale to highlight its slow convergence to the low density limit of 1. The slow convergence is caused by the predominance of the $\Lambda(1405)$ resonance for densities roughly below $0.06\rho_0$ where this ratio exhibits hump structure with values exceeding 1, owing to the large negative values assumed by $\text{Re } \tilde{f}_{I=0}$ near threshold in Eq. (5). At densities above $0.06\rho_0$, the shown ratio decreases monotonically with density from a value 1 owing to the rapid increase of $\text{Re } \tilde{f}_{I=0}$ below 1415 MeV (where the $\Lambda(1405)$ resonates as far as f is concerned) and levels off when $\text{Re } \tilde{f}_{I=0}$ has reached its (positive) maximum value. Thus, although the effect of the $\Lambda(1405)$ subthreshold resonance appears to be limited to low densities, it affects implicitly the absorptivity $\text{Im } \mathcal{F}_{K^-N}(\rho)$ at densities higher than $\approx 0.1\rho_0$, cutting it to less than half of the free-space input absorptivity $\text{Im } f_{K^-N}(\rho)$. The resulting $\text{Im } \mathcal{F}_{K^-N}(\rho)$ which is induced by $K^-N \rightarrow \pi Y$ pionic absorption is totally insufficient in kaonic atoms fits and needs to be supplemented by non-pionic absorptive contributions.

The second piece of the K^- nuclear potential is a phenomenological $V_{K^-}^{(2)}$, simulating two-nucleon ($2N$) dispersive and absorptive $K^-NN \rightarrow YN$ processes and multi-nucleon processes. It is parametrized by

$$V_{K^-}^{(2)} = -(4\pi/2\mu_K)[b\rho + B\rho(\rho/\rho_0)^\alpha], \quad (7)$$

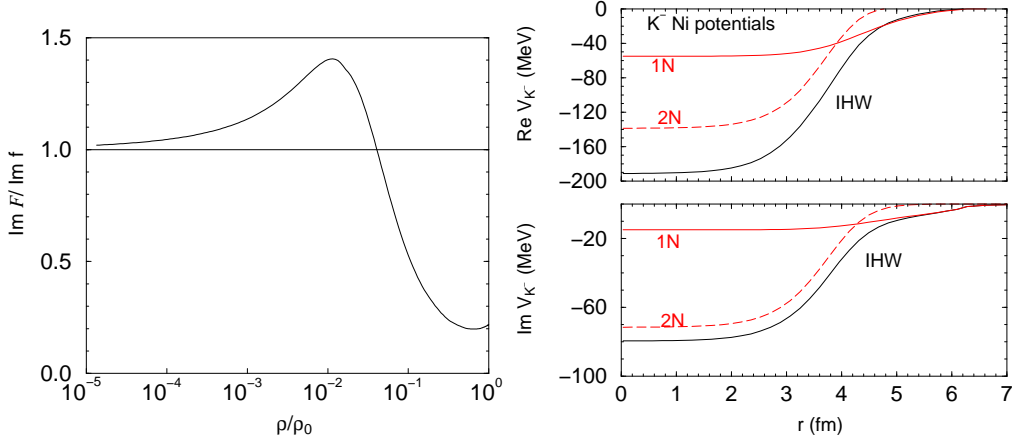


Figure 3: Left: ratio of $\text{Im } \mathcal{F}_{K-N}(\rho)$ to $\text{Im } f_{K-N}(\rho)$ calculated as a function of nuclear density in Ni for the IHW amplitudes in the absence of the $V_{K^-}^{(2)}$ potential term. Right: $1N$ and $2N$ components of the IHW-based kaonic atom potential in Ni.

where μ_K is the kaon-nucleus reduced mass, b and B are two complex parameters and the real exponent α satisfies $\alpha > 0$. Constraining $\text{Im } V_{K^-}^{(2)}$ to be non-negative at all values of ρ by imposing $\text{Im } b=0$ and gridding on α , the following values are obtained in a best-fit search:

$$b = (-0.34 \pm 0.07) \text{ fm}, \quad B = (1.94 \pm 0.16) + i(0.83 \pm 0.16) \text{ fm}, \quad \alpha = 1.2. \quad (8)$$

The contribution of this fitted $V_{K^-}^{(2)}$ to the kaonic atoms potential is substantial for densities larger than $\approx 0.5\rho_0$ where it exceeds the contribution of the IHW-based $V_{K^-}^{(1)}$, as clearly seen on the r.h.s. of Fig. 3. The plotted $1N$ potential corresponds to a situation where $V_{K^-}^{(2)} = 0$, but in the final $1N+2N$ potential the $1N$ component is affected by the $2N$ component due to the implicit coupling between the two in the self consistent procedure related to Eq. (4). A non-additivity of the two components in the final potential is observed, particularly for the imaginary potential.

Several other fitted kaonic atom potentials are compared to the IHW-based ($1N+2N$) potential in Table 2. The DD potential is a purely phenomenological potential of a form similar to Eq. (7) and offers a benchmark, with $\chi^2=103$, for what may be viewed as the ultimate density dependent fit to 65 data points across the periodic table (it was denoted *nominal* in Ref. [28]). The entry for the NLO30 model is typical of results obtained in Refs. [23, 24].

Table 2: Properties of K^- -Ni potentials from global fits to 65 kaonic atom data points. Values of potentials are in MeV, r.m.s. radii in fm.

model	χ^2	$V_R(0)$	$V_I(0)$	r_R	r_I	α
DD [28]	103	- 199	-76	3.48	3.71	0.25
IHW [21]	118	- 191	-79	3.34	3.73	1.2
NLO30 [24]	148	- 179	-71	3.42	3.70	1.0

All three displayed fits produce deeply attractive real potentials, with depth in the range 180–200 MeV at the center of Ni, and sizable absorptivities measured by imaginary potential depths in the range 70–80 MeV. The r.m.s radii of V_R are all smaller significantly than the point-proton distribution r.m.s. radius $r_p=3.69$ fm in Ni, reflecting the sizable contribution of the more compact $\text{Re } V_{K^-}^{(2)}$, whereas the r.m.s radii of V_I are all slightly larger than r_p , reflecting the compensating effect of $\text{Im } V_{K^-}^{(2)}$ on the rapidly decreasing with density $\text{Im } V_{K^-}^{(1)}$. The very significant improvement of 30 units in χ^2 values by going from NLO30 to IHW is due to species where strong interaction observables were measured for more than a single kaonic atom level. The width (or equivalently ‘yield’) of the upper level is normally dominated by $\text{Im } V_{K^-}^{(1)}$, whereas the width of the lower level is dominated by $\text{Im } V_{K^-}^{(2)}$. **Thus, more accurate determination of two level widths in the same kaonic atom are likely to pin down the density dependence of $\text{Im } V_{K^-}^{(2)}$ as it evolves with density and overtakes $\text{Im } V_{K^-}^{(1)}$.** The range of nuclear densities which prove to be effective for absorption from the lower level is exhibited on the l.h.s. of Fig. 4 for Ni by plotting overlaps of the $4f$ atomic radial wavefunction squared with the Ni matter density ρ_m for two choices of V_{K^-} [29]; see also Refs. [30, 31]. The figure demonstrates that, whereas this overlap for the relatively shallow, density-independent $t\rho$ potential peaks at nuclear density of order 10% of ρ_0 , it peaks at about 60% of ρ_0 for the deeper, density-dependent DD potential and has a secondary peak well inside the nucleus (indicating that a K^- nuclear $\ell = 3$ quasibound state exists). The DD potential, clearly, exhibits sensitivity to the interior of the nucleus whereas the $t\rho$ potential exhibits none. **The superiority of Deep to Shallow V_{K^-} can be checked by devising new measurements in a few carefully selected kaonic atoms [32].**

A reaction that could discriminate between deep and shallow K^- nuclear

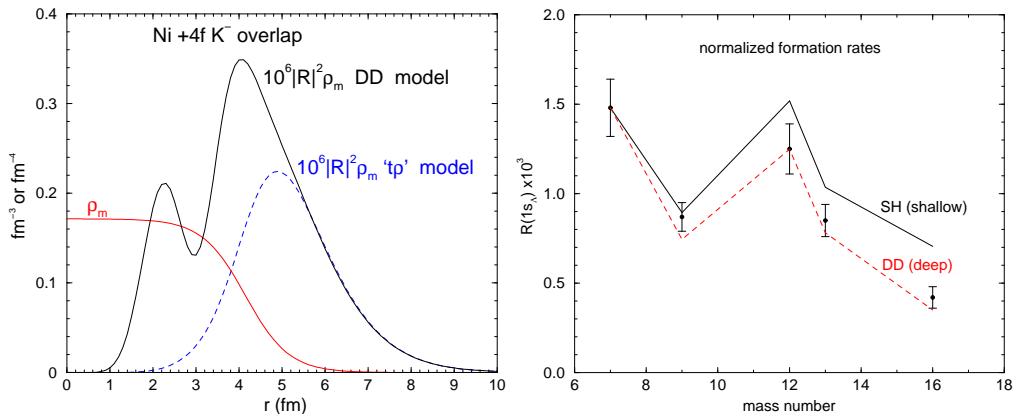


Figure 4: Left: overlap of K^- -Ni atomic $4f$ radial wavefunction R squared with Ni matter density ρ_m in two models [29]. Right: $1s_\Lambda$ formation rates per K^-_{stop} from K^- capture at rest spectra taken by FINUDA [33] and as calculated [34] – normalized to the ${}^7_\Lambda\text{Li}$ datum – using in-medium density dependent $K^-n \rightarrow \pi^- \Lambda$ branching rates that relate subthreshold energies to densities similarly to Eq. (4).

potentials is the K^- capture at rest formation of Λ hypernuclear states localized in the nuclear interior. The formation rates are expected to be sensitive to the extent to which the relevant K^- atomic wavefunctions penetrate into the nucleus. Spectra and formation rates of several p -shell hypernuclei were reported recently by the FINUDA experiment [33] and analyzed by Cieplý et al. in Ref. [34]. A comparison between experiment and calculation is shown on the r.h.s. of Fig. 4. The calculations use in-medium subthreshold $K^-n \rightarrow \pi^- \Lambda$ branching rates where the density dependence is related to the subthreshold energy according to Eq. (4). **This comparison favors deep potentials to shallow ones.**

Attempts to evaluate the absorptivity $\text{Im } V_{K^-}^{(2)}$ in addition to $\text{Im } V_{K^-}^{(1)}$ within a chiral unitary approach have been reported by Sekihara et al. [35]. Their calculated nuclear-matter potentials, as a function of nuclear density ρ_N , are shown in Fig. 5 for several values of the K^- momentum p_K between 0 to 250 MeV/c. The higher p_K is, the deeper the K^-N related amplitudes bite into the subthreshold region, which weakens both $1N$ and $2N$ absorptivities, in agreement with the lessons gained in Refs. [21, 23, 24, 26]. To establish correspondence with finite nuclei, these authors determined the local densities probed for the chosen values of p_K by offsetting the K^- kinetic energy

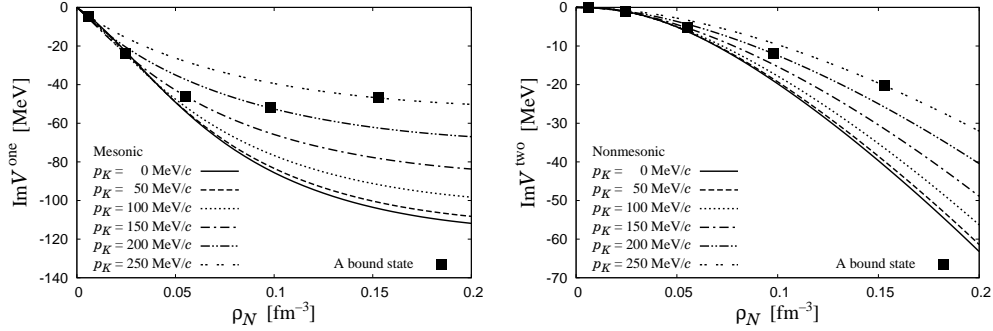


Figure 5: $\text{Im } V_{K^-}^{(1)}(\rho_N)$ (left) and $\text{Im } V_{K^-}^{(2)}(\rho_N)$ (right) evaluated in nuclear matter within a chiral unitary approach [35] for several values of the K^- momentum p_K . The filled squares denote the density ρ_N corresponding to p_K , see text.

$p_K^2(\rho_N)/2m_K$ against a prescribed potential $V_{K^-}(\rho_N) = -70 \text{ MeV} \times (\rho_N/\rho_0)$, resulting in values of density ρ_N marked by filled squares in the figure. The finite-nucleus absorptivities are then obtained by connecting smoothly these filled squares. Comparing these calculated absorptivities at nuclear central density $\rho_0 \approx 0.16 \pm 0.01 \text{ fm}^{-3}$ with the IHW-based absorptivities shown for Ni in the lower r.h.s. of Fig. 3, one observes that $\text{Im } V_{K^-}^{(1)}$ is overestimated by over a factor of two whereas $\text{Im } V_{K^-}^{(2)}$ is underestimated by over a factor of three. As a consequence, the ratio of $\text{Im } V_{K^-}^{(2)}/\text{Im } V_{K^-}^{(1)}$ plotted in Fig. 17 of Sekihara et al. [35] underestimates significantly the relative strength of K^- multinucleon absorption (occurring at $\rho \lesssim 0.5\rho_0$) as compared to indications from old emulsion and bubble-chamber work [36].

4. Many-body kaonic quasibound states

The state of the art in K^- quasibound states calculations in nuclear systems beyond four-body systems has been reviewed recently, and also in these proceedings, by Jiří Mareš [26]. For the sake of completeness, I show in Fig. 6 results borrowed from his presentation summarizing self consistent calculations of K^- quasibound states in nuclei ranging from ${}^4\text{He}$ to ${}^{208}\text{Pb}$. A prominent feature resulting from the imposition of self consistency on these calculations is the hierarchy of widths calculated within a given nucleus. With energy independent potentials one expects the width to be maximal for the lowest, most localized $1s_K$ states, and to monotonically decrease for

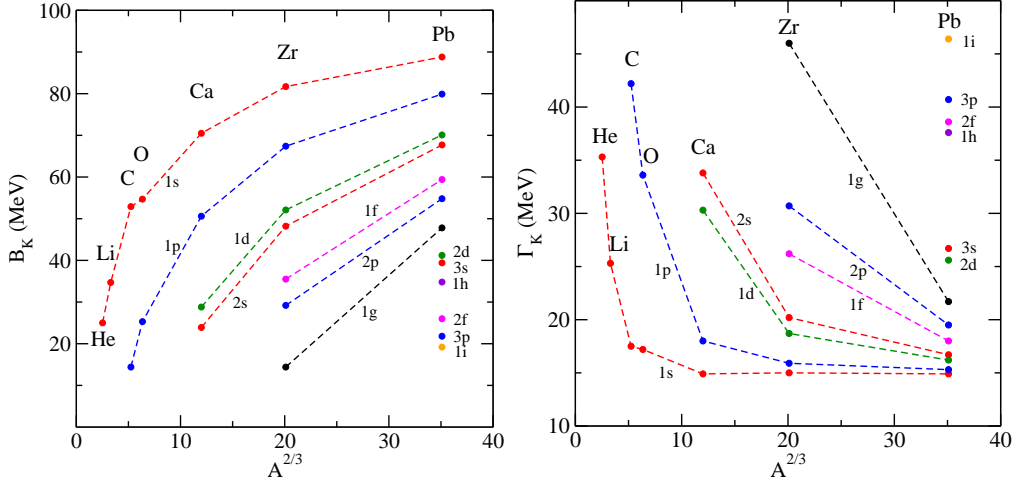


Figure 6: Binding energies B_K (left) and widths Γ_K (right) of K^- quasibound states in selected nuclei calculated self consistently by Gazda and Mareš [26] using static RMF densities and NLO30 in-medium K^-N subthreshold amplitudes, but without any $V_{K^-}^{(2)}$ contribution.

excited states which are less localized within the core nucleus. The reverse is observed on the r.h.s. of the figure. This arises by requiring self consistency: the more excited a K^- quasibound state is, the lower nuclear density it feels, and a smaller downward shift into subthreshold energies is implied by the s_ρ dependence. Since $\text{Im } V_{K^-}^{(1)}$ decreases strongly below threshold, this means that its contribution gets larger, the higher in energy the excited quasibound state is. As stressed by Gazda and Mareš [26], **the large widths coupled with smaller excitation energy spacings should make it difficult to identify experimentally such K^- quasibound states in a unique way. Additional width contributions from $\text{Im } V_{K^-}^{(2)}$ will only compound this difficulty.**

5. $\Sigma^*(1385)N$ vs. $\Lambda^*(1405)N$

The $I = 1/2$, $J^\pi = 0^-$ K^-pp quasibound state discussed in Sect. 2 represents a close realization of a Λ^*N quasibound 1S_0 dibaryon [37]. Similarly, one could ask whether Σ^*N dibaryon quasibound states are realized and, if so, for which quantum numbers. A close realization of a Σ^*N quasibound 5S_2 dibaryon in terms of $I = 3/2$, $J^\pi = 2^+$ πYN quasibound state \mathcal{Y} was

proposed a few years ago and established more solidly in the recent work of Ref. [5] within a relativistic three-body Faddeev calculation some 10–20 MeV below the $\pi\Sigma N$ threshold. The leading two-body attractive channels in this three-body system are the p -wave πN and $\pi\Lambda - \pi\Sigma$ channels dominated by the $\Delta(1232)$ and $\Sigma(1385)$ resonances, respectively, and to a lesser extent the 3S_1 YN s -wave channel. It was found that admixing a $\bar{K}NN$ channel to the πYN three-body channels affects little this dibaryon quasibound state since for a p -wave \bar{K} meson it requires a Pauli forbidden $I_{NN} = 1, S_{NN} = 1$ combination for the leading NN s -wave configuration.

This dibaryon candidate \mathcal{Y} may be looked for in experiments similar to those being run at GSI [38] and J-PARC [39] which aim at observing the associated production of K^-pp and its subsequent decay to a Λp pair. Thus, at GSI one could look for

$$\begin{aligned}
 p + p &\rightarrow \mathcal{Y}^{++} + K^0 \\
 &\hookrightarrow \Sigma^+ + p,
 \end{aligned}
 \tag{9}$$

where the decay $\mathcal{Y}^{++} \rightarrow \Sigma^+ p$ offers a unique decay channel, and at J-PARC look for

$$\begin{aligned}
 \pi^\pm + d &\rightarrow \mathcal{Y}^{++/-} + K^{0/+} \\
 &\hookrightarrow \Sigma^\pm + p(n),
 \end{aligned}
 \tag{10}$$

where again these decay channels offer unique channels distinctly from those looked for in K^-pp searches.

Acknowledgments

Special thanks are due to Nir Barnea, Aleš Cieplý, Eli Friedman, Humberto Garcilazo, Daniel Gazda and Jiří Mareš, with whom I have collaborated on topics surveyed here, and to Wolfram Weise for many ongoing stimulating discussions and kind hospitality at TUM in recent years.

References

- [1] SIDDHARTA Collaboration: M. Bazzi, et al., Phys. Lett. **B704** (2011) 113, Nucl. Phys. **A881** (2012) 88.
- [2] T. Hyodo, Nucl. Phys. **A914** (2013) 260, particularly Fig. 2.

- [3] S. Wycech, Nucl. Phys. **B28** (1971) 541.
- [4] W.A. Bardeen, E.W. Torigoe, Phys. Lett. **B38** (1972) 135.
- [5] A. Gal, H. Garcilazo, Phys. Rev. **D78** (2008) 014013; H. Garcilazo, A. Gal, Phys. Rev. **C81** (2010) 055205, Nucl. Phys. **A897** (2013) 167.
- [6] A. Gal, Int. J. Mod. Phys. **E19** (2010) 2301 [SNP2008]; A. Gal, Chin. Phys. **C34** (2010) 1169 [QNP2009]; W. Weise, Nucl. Phys. **A835** (2010) 51 [HYP2009]; T. Hyodo, Few-Body Systems **54** (2013) 931 [FB2012].
- [7] N. Barnea, A. Gal, E.Z. Liverts, Phys. Lett. **B712** (2012) 132.
- [8] A. Doté, T. Hyodo, W. Weise, Nucl. Phys. **A804** (2008) 197, Phys. Rev. **C79** (2009) 014003
- [9] Y. Ikeda, H. Kamano, T. Sato, Prog. Theor. Phys. **124** (2010) 533.
- [10] T. Yamazaki, Y. Akaishi, Phys. Lett. **B535** (2002) 70.
- [11] N.V. Shevchenko, A. Gal, J. Mareš, Phys. Rev. Lett. **98** (2007) 082301, Phys. Rev. **C76** (2007) 044004 (with J. Revai).
- [12] Y. Ikeda, T. Sato, Phys. Rev. **C76** (2007) 035203, **C79** (2009) 035201.
- [13] S. Wycech, A.M. Green, Phys. Rev. **C79** (2009) 014001.
- [14] T. Hyodo, W. Weise, Phys. Rev. **C77** (2008) 035204.
- [15] Y. Kanada-En'yo, D. Jido, Phys. Rev. **C78** (2008) 025212.
- [16] Y. Akaishi, T. Yamazaki, Phys. Rev. **C65** (2002) 044005.
- [17] T. Yamazaki, A. Doté, Y. Akaishi, Phys. Lett. **B587** (2004) 167.
- [18] D. Gazda, E. Friedman, A. Gal, J. Mareš, Phys. Rev. **C80** (2009) 035205, and references therein.
- [19] M. Bayar, E. Oset, Nucl. Phys. **A914** (2013) 349, and references therein.
- [20] N.V. Shevchenko, Nucl. Phys. **A890-891** (2012) 50, **A914** (2013) 321.
- [21] E. Friedman, A. Gal, Nucl. Phys. **A899** (2013) 60.

- [22] Y. Ikeda, T. Hyodo, W. Weise, Phys. Lett. **B706** (2011) 63, Nucl. Phys. **A881** (2012) 98.
- [23] A. Cieplý, E. Friedman, A. Gal, D. Gazda, J. Mareš, Phys. Lett. **B702** (2011) 402, Phys. Rev. **C84** (2011) 045206.
- [24] E. Friedman, A. Gal, Nucl. Phys. **A881** (2012) 150.
- [25] A. Cieplý, J. Smejkal, Nucl. Phys. **A881** (2012) 115, & cited refs.
- [26] D. Gazda, J. Mareš, Nucl. Phys. **A881** (2012) 159, **A914** (2013) 326.
- [27] T. Waas, M. Rho, W. Weise, Nucl. Phys. **A617** (1997) 449.
- [28] E. Friedman, A. Gal, C.J. Batty, Nucl. Phys. **A579** (1994) 518.
- [29] E. Friedman, A. Gal, in *From Nuclei to Stars, Festschrift in Honor of Gerald E. Brown*, Ed. Sabine Lee (WS 2011) pp. 127–140.
- [30] N. Barnea, E. Friedman, Phys. Rev. **C75** (2007) 022202.
- [31] J. Yamagata, S. Hirenzaki, Eur. Phys. J. **A31** (2007) 255.
- [32] E. Friedman, Int. J. Mod. Phys. **A26** (2011) 468.
- [33] M. Agnello, et al., Phys. Lett. **B698** (2011) 219.
- [34] A. Cieplý, E. Friedman, A. Gal, V. Křečičířík, Phys. Lett. **B698** (2011) 226.
- [35] T. Sekihara, J. Yamagata-Sekihara, D. Jido, Y. Kanada-En'yo, Phys. Rev. **C86** (2012) 065205.
- [36] C. Vander Velde-Wilquet, J. Sacton, J.H. Wickens, D.N. Tovee, D.H. Davis, Nuovo Cimento **39A** (1977) 538, and references therein.
- [37] T. Uchino, T. Hyodo, M. Oka, Nucl. Phys. **A868-869** (2011) 53.
- [38] L. Fabbietti, et al., Nucl. Phys. **A914** (2013) 60, and references therein.
- [39] T. Takahashi, Nucl. Phys. **A914** (2013) 530, and references therein for J-PARC E27 (search for K^-pp in $d(\pi^+, K^+)$, T. Nagae spokesperson).